Structural Regime Identification in Ionotropic Alginate Gels: Influence of the Cation Nature and Alginate Structure

Pierre Agulhon, Mike Robitzer, Laurent David, Françoise Quignard

Structural Regime Identification in Ionotropic Alginate Gels: Influence of the Cation Nature and Alginate Structure

Pierre Agulhon,[†] Mike Robitzer,[†] Laurent David,[‡] and Françoise Quignard*[,†]

[†]Institut Charles Gerhardt Montpellier, UMR 5253 CNRS-UM2-ENSCM-UM1, Matériaux Avancés pour la Catalyse et la Santé, ENSCM, 8 rue de l'Ecole Normale, 34296 Montpellier cedex 5, France

[‡]Université de Lyon, Institut de Chimie de Lyon FR 3023, Université Claude Bernard Lyon 1, Ingénierie des Matériaux Polymères CNRS UMR 5223, IMP@Lyon1, Ecole Polytechnique Universitaire de Lyon 1, 15 bd Latarjet, F-69622 Villeurbanne Cedex, France

ABSTRACT: The morphologies of several ionotropic alginate hydrogels and aerogels were investigated by SAXS according to the nature of the divalent metal cation (Mn2+,Co2+,Zn2+, Cu2+) and the guluronic fraction of the alginate. All alginate hydrogel and aerogel samples show isotropic small-angle X-ray scattering. Gelation results from cooperative associations of cations and chain segments and yields different nanostructures, that is, nanofibrillar morphology or multiple junction morphology, according to cation type and eventually mannuronic/guluronic ratio. Therefore, Mn and Cu gels present the same morphology whatever the guluronic ratio, whereas Co and Zn gels yield different nanostructures. In the size range investigated by SAXS (~10−200 Å), the structure of aerogels obtained by CO2 supercritical drying is found to be inherited from the morphology of the parent hydrogel whatever the initial structural regime.

INTRODUCTION

Alginates are natural polysaccharides produced by brown algae,[1] composed of (1−4)-linked uronate residues (pyranose rings with a carboxylic group in C-6) (Figure 1). β-D-Mannuronate and α-L-guluronate residues are present in varying proportion, sequence, and molecular weight.[2−4] The axial orientation of the (1−4)-links of the guluronate residues and equatorial in the case of mannuronate account for variations of the organization and stability of the ionotropic gels formed by alginates with different mannuronic/guluronic (M/G) ratios.

Alginates are able to form heat-stable strong gels with divalent or trivalent cations (except Mg^{2+}), whereas monovalent metal ions form soluble salts. This property is the basis for applications of alginates in drug release systems[5] and as supports in biocatalysis. Cations show different affinity for alginate. The interaction of the polyuronate chains with various divalent cations has been monitored by circular dichroism (c.d.).[6−8] Spectral change when gelation is induced by Cu^{2+} suggested a nonspecific binding mechanism, consistent with the lack of selectivity of Cu^{2+} for different polyuronates.[9,10]

The influence of the nature of the divalent cations on the network elasticity was demonstrated by calorimetric and dilatometric methods. The Young modulus of the gels followed the order Cd > Ba > Cu > Ca > Ni > Co > Mn. There is a linear relation between the observed values of the Young modulus and the logarithm of the association constant for divalent cations-alginate complexes.[11,12] Alginates with high guluronic content give gels with a higher strength than alginate with low guluronic content. This was attributed to the stronger affinity of the guluronic residues for divalent cations.[13−15] The effects of metal ion complexation on the morphology of the resultant gels were evaluated by polarized optical microscopy and electron microscopy.[16−18] Alginates can also form acidic gel by lowering the pH of a sodium alginate solution.[5,19] Acidic gels, like ionotropic gels, present a higher mechanical strength for a high guluronic content. Small-angle X-ray scattering (SAXS) suggested the formation of junction zones with a high degree of multiplicity. In the case of calcium or acidic hydrogels, SAXS experiments were performed on gels obtained by slow release of gelling agent.[20,21] Draget et al. showed that the two gel systems could not be described by a simple monodisperse rod-like model and multiplicity of junction zone nature should be taken into account.[22,23] Calcium induces gelation with polymer chains aggregated to form rod-like structures with cross-sectional radii of the order of 10 to 20 Å.[23,24] Acidic gels show larger aggregated structures (size ~50 Å). M and G sequences both contribute to cooperative aggregation, and MG alternated structures favor solubility at all pH values. In a previous study, we demonstrated the interest of a structural study in the case of calcium−alginate hydrogels systems to predict the morphology of the corresponding

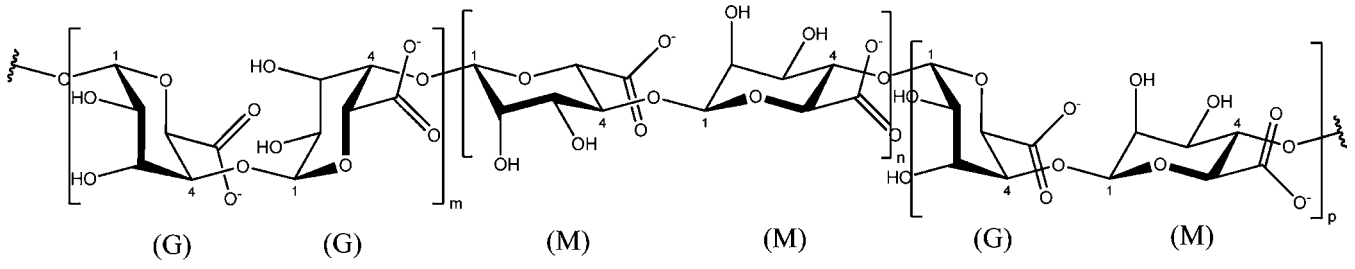

Figure 1. Structural units of alginate. M: mannuronate residue; G: guluronate residue.

aerogels. The SAXS patterns exhibited an asymptotic behavior at low-q values (in the experimental q range 7×10^{-3} to 2×10^{-2} Å^{-1}) close to $I(q) \approx q^{-1}$, which was indicative of rod-like scattering objects with random orientation. The evolution of the diameter of such rod-like objects was thus deduced from the maxima observed on Kratky plots, that is, $I(q)\cdot q^2$ versus q. The results were in perfect agreement qualitatively (rod-like anisometry type of the scattering objects) and quantitatively (diameter of the rods) with direct SEM observations of the morphology of aerogels and with the results of N_2 adsorption on the aerogel. This was evidence that under the experimental conditions chosen, the nanostructure of the aerogel depends on the morphology of pre-existing rod-like objects within the gel, that is, that the structure of the aerogel provided a correct image of the structure of the parent gel.[25]

Recent developments for cleaner sustainable chemistry are being driven by a shift from petrochemical-based feedstocks to biological materials. There is indeed a considerable interest in exploiting natural polymer macrostructures, and, in particular, those from polysaccharides, to create high-performance and environmentally friendly catalysts. Nevertheless, the introduction of renewable resources in the production of catalyst supports and adsorbents is only possible if the materials intended to replace oil-derived or energy-intensive solids present adequate properties, such as high surface area, appropriate surface chemistry and porosity, thermal and chemical stability, and low cost. Algal polysaccharides, for the economics of their growth and their ease of extraction, are classed among the less-energy consuming alternatives to fossil fuels.[1,26] As far as remediation and heterogeneous catalysis are concerned, diffusion properties and high surface areas are common requisites. Aerogel formulations of ionotropic alginate gels fulfill the textural requisites,[27] and metal transition cations are of prime interest for catalytic purposes. In this work, the morphologies of alginate hydrogels and aerogels are investigated by SAXS, according to the nature of the divalent cation and the guluronic fraction of the alginate. The textural properties of the aerogels are discussed in relation to the SAXS patterns.

MATERIALS AND METHODS

Ionotropic Alginate Gels Synthesis. Alginate samples were supplied by FMC Biopolymer (Norway) and characterized by ^{1}H NMR according to Grasdalen.[28,29] According to their respective guluronate content, alginates were designated as HG and LG for "high G" and "low G". The percents of guluronate unities in the alginate backbone were 63 and 33, respectively (complete characterization reported in Table 1 of the Supporting Information).

Hydrogel millimetric beads were obtained by dropwise addition of a 2% sodium alginate solution (10 mL) into a gelling solution prepared with divalent cation chloride salt (0.1 mol·L^{-1}, 10 mL). After formation, the beads were left in gelling medium for 3 h. Alcogels were formed by stepwise solvent exchange: the hydrogel microspheres were dehydrated by immersion in a series of successive ethanol−water baths of increasing alcohol concentration (10, 30, 50, 70, 90, and 100%) for 15 min each. Ethanol was replaced by liquid CO_2, which was eliminated in a Polaron 3100 apparatus under supercritical conditions beyond 31 °C and 74 bar (typically 39 °C and 85 bar) leading to the aerogel spheres. The same procedure was followed for acidic gels using a 1 mol·L^{-1} hydrochloric acid gelling solution. To avoid any morphological differences due to depressurization conditions, the 12 samples described were dried together.

Characterization. Nitrogen adsorption isotherms at −196 °C were recorded on a Micromeritics Tristar apparatus. Prior to the analysis, the aerogel samples were outgassed at 50 °C under dynamic vacuum. The volume of the adsorbed monolayer was evaluated by the BET equation, and the surface area was calculated by assuming a N_2 molecule to cover 0.162 nm^2.

Scanning electron microscopy (SEM) pictures were recorded on a Hitachi S-4800 microscope after platinum metallization.

The SAXS data were collected on BM2-D2AM beamline at the European Synchrotron Radiation Facility (Grenoble, France) 9 days after the preparation of the samples. The data were collected at incident photon energy of 16 keV, the synchrotron working in 16-bunch mode. A bidimensional detector (CCD camera from Ropper Scientific) was used. The sample holders were metallic disks (diameter 10 mm, thickness 2 mm) with a central hole where the microspheres were placed. All data corrections were performed by the software bm2img available on the D2AM beamline. The data were corrected for dark image (response of the camera with no incident beam), flat field response (obtained after illumination of the camera with a fluorescent sample), and geometrical image distortion of the camera. Finally, the radial average around the image center (location of the center of the incident beam) was performed for the q-range calibration standard (silver behenate) and the studied samples. The scattering data are normalized by the transmitted intensity so that the scattering pattern of the empty cell can be subtracted from all other scattering diagrams.

RESULTS AND DISCUSSION

Dropwise addition of 2% w/w sodium alginate solution into the various gelling media leads to hydrogel beads formation whatever the cation used. Alginate beads are mechanically stable and the solvent exchange to alcogel or the supercritical drying does not change the macroscopic shape of the samples. (See Figure 2.)

Metal loading of each system is investigated through thermogravimetric studies of aerogel samples and allow estimating the number of uronate units per cation (Supporting Information, Table 2). Aerogel calcination under an air atmosphere leads to the corresponding oxide formation.[30] At 900 °C, all of the organic part is eliminated, and the residual mass is only due to the oxide of the gelling cation. The number of uronate units per cation is not very precise, but it allows some qualitative conclusions. Therefore, for each alginate and each cation this ratio is close to 2, which is the theoritical value for total complexation with divalent cations. Along with the absence of sodium in the oxide (determined by EDX), this

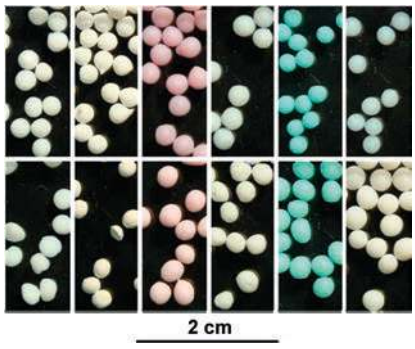

Figure 2. Aerogel beads of alginate HG (upper range) and alginate LG (lower range) with various gelling conditions: Acidic, Mn^{2+}, Co^{2+}, Zn^{2+}, Cu^{2+}, and Ca^{2+} from left to right, respectively.

result confirms that each uronate unit (M or G) participates in the complexation when using an excess of gelling cation. The slight deviation from 2 (1.9 ± 0.1) may be due to a little part of acidic gelation[31] with cation solution pH ranging from 4 to 6 (the pK_a of guluronic and manuronic acids is close to 3.45), but it is not clearly alginate depending.

Nanostructure of Hydrogels and Aerogels. All alginate hydrogel and aerogel samples show isotropic small-angle X-ray scattering. Plots of scattered intensities averaged along azimutal angles versus the scattering vector q in log−log scale for hydrogel and aerogel samples are displayed in Figure 3. For a

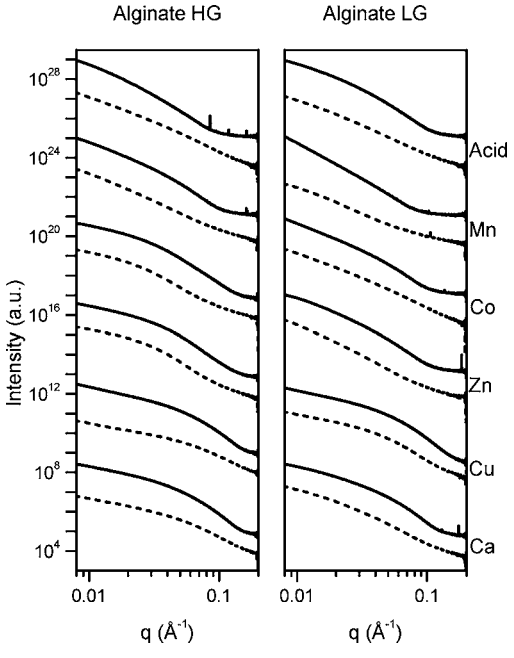

Figure 3. Small-angle X-ray scattering profiles for aerogel (solid lines) or hydrogel (dashed lines) samples obtained with alginate HG (on the left) or alginate LG (on the right). For clarity, the curves of each cation are arbitrary shifted up by successive 10 000 factors, but the relative intensity between an aerogel and the corresponding hydrogel is kept unchanged.

given cation and a given alginate, the scattering pattern is little affected by the gel physical state: hydrogel or aerogel as previously reported for calcium HG-alginate gel.[25] Except for alginate LG with manganese, aerogel shows the same scattering behavior type as the corresponding hydrogel (at least in low-q range). The only difference concerns the relative intensity due to the different contrast between the gel and the solvent (water or air).

The SAXS patterns can be divided in two main ranges, analyzing the intensity data according to

$$I(q) \approx A/q^{\alpha}$$

In the q range $0.03 < q < 0.1$ Å^{-1} (Figure 4), the slope of the log−log plot, that is, the scattering exponent α, stays between

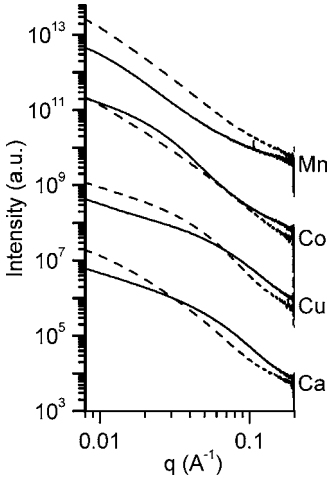

Figure 4. SAXS patterns of hydrogel samples obtained with alginate HG (solid line) or alginate LG (dashed line) with different cations. For clarity, the curves of each cation are arbitrary shifted up by successive 100 factors, and the relative intensity for a given cation is kept unchanged.

−4 and −5 for aerogel samples and ranges from −3 to −4 for hydrogel samples. At lower q values ($q < 0.03$ Å^{-1}), the scattering exponent is lower and ranges from −1 to −4 according to the investigated system. The low-q scattering exponents were determined by least-squares fits (Supporting Information, Table 3). This analysis was kept even for acidic or manganese hydrogels where the separation of the scattering diagram into two well-apparent q ranges may not be obvious.

The scattering behavior observed in the low-q range (Supporting Information, Table 3) enables us to evidence two structural organizations in hydrogels. Mn-alginate systems exhibit a high scattering exponent value α (above 2), whereas Cu and Ca cations yield hydrogel structures with an α value below 2. As discussed by Draget et al.,[32] such behavior is indicative of a fine fibrillar morphology when α is close to 1 (Ca-LG and Ca-HG; Cu-LG and Cu-HG; Zn-HG and Co-HG) and a more complex morphology with junction nature multiplicity when α is higher than 2 (H-HG and H-LG; Mn-LG and Mn-HG; Zn-LG and Co-LG).

The case of Zn and Co hydrogels systems has also to be discriminated because the structural regime depends on the type of alginate: High guluronic alginate (HG) induces the formation of the fibrillar organization, whereas low guluronic alginate (LG) induces the formation of junctions with multiple morphologies.

As for previous studies, calcium and acidic gels seem to have different behaviors. Acidic gels show a stronger initial slope along with a smoother transition with the second part of the scattering pattern. For the investigated transition-metal cations (Mn, Co, Zn, Ca, and Cu), we can classify each sample in two

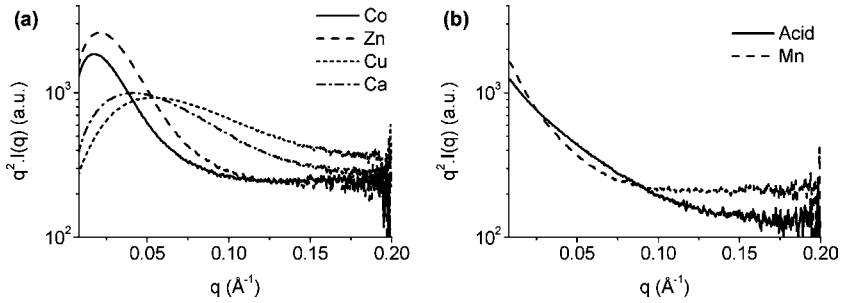

Figure 5. Kratky plot of alginate HG hydrogel samples with various cations: (a) calcium-type with fibrillar morphology and (b) acidic-type with multiple junction morphology.

categories whether its low-q slope is higher or lower than −2, that is, whether it displays the scattering behavior of acidic-alginate hydrogel or calcium-alginate hydrogel. This classification reveals in fact a third category comprising the samples behaving like calcium with alginate HG and like acidic gel with alginate LG. Therefore, with cobalt and zinc, the guluronic fraction impacts the hydrogel morphology because scattering patterns with "calcium-type" shape or "acidic-type" shape with alginate HG or LG, respectively, are obtained. On the contrary, with both alginates, manganese always shows an acidic behavior, whereas copper exhibits a calcium behavior.

To go a step further in the investigation of the nanostructure (i.e., secondary structure) of hydrogels, we tested in more detail the rod-like approximation by means of Kratky plots (i.e., $q^2 \cdot I(q)$ vs q plots) as shown in Figure 5. The scattering behavior of a collection of randomly oriented rods should exhibit a maximum at $q \approx 1/R_c$, where R_c is the mean gyration radius in the cross-section of the rods. The outer radius of the fibrils is then given by $R_0 \approx R_c\sqrt{2}$. The results for the diameter of the fibrils $d \approx 2R_0 = 2R_c\sqrt{2}$ are gathered in Table S4 in the Supporting Information.

In agreement with the published interpretation,[32] the differences in morphology result from the cooperative interactions between the metallic cations and mannuronic and guluronic sequences within the primary structure of alginates. Complexation of cations do not depend on the guluronic content of alginate, as shown by Table 2 of the Supporting Information, but the structuration resulting from cooperative associations of several macromolecular chains is shown to depend on the nature of the cation or the structure of the alginate chain. Copper cations seem to interact strongly with both mannuronic and guluronic residues and induce a comparable fibrillar morphology whatever the guluronic content. The scattering exponents are significantly impacted by alginate type in calcium-alginate hydrogels, and thus calcium cations seem to induce chain associations into fibrils preferentially with guluronic residues. A clear transition in the morphology is observed from HG to LG for cobalt and zinc hydrogels, which again should be due to a decrease in the cooperative interaction effects for LG systems. Mn and acidic hydrogels display the nonfibrillar morphology that could be due to an absence of cooperative interchain associations for all investigated alginate types. The morphology of aerogel samples, as deduced by SAXS, was shown to be mainly inherited for the parent morphology of corresponding hydrogels for calcium-alginate gels.[25] In this work, we observed the same trends for a variety of cations for two alginate systems. This resulted in similar values of the power exponents α characterizing the morphology type of hydrogels and their corresponding aerogels. The main differences between metallic cation-alginate systems would thus lie in the molecular organization within the junction zones, where fibrillar or more complex junctions with multiple natures could be found.

To gain more insight into the role of the metal cation-uronic unit interactions, quantum chemical calculations on the model complex structures are in progress. Quantitative information about the local structure of the complexes as a function of the chemical nature of the cation and the uronic G or M unit are expected. Indeed, in the case of Ca^{2+}, molecular dynamics simulation revealed that changes in the ion-binding mode must play a rule in chain−chain association within junction zones and in the stiffening of the chains.[33,34] This effect is expected to be even more pronounced for transition-metal ions.

Relation of the Textural Properties and the Nanostructure of Aerogel. SEM on the cross-section of aerogel beads reveals a macroporous texture. Interconnected fibers form a 3D network as shown in Figure 6. This morphology is

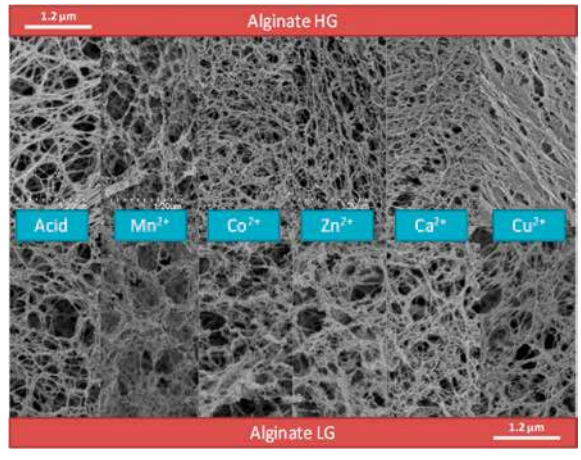

Figure 6. SEM picture of M-alginate HG and LG aerogel (same scale for all images).

observed in each sample with slight differences in the network density and the roughness of the fibers.

The fibrillar network of aerogel beads leads to high surface areas as determined by the analysis of the N_2 adsorption−desorption isotherm at 77 K.[35] The shape of adsorption−desorption isotherm of N_2 at 77 K is typical of a type IV isotherm in the classification of the IUPAC[36] with a strong adsorption at low relative pressure and a hysteresis loop at very high relative pressure. This behavior characterizes large mesopores and macropores. The application of the α_S method indicates that the solid does not present micropores. The broad

size distribution of the mesopores is centered around 30−40 nm.

The range of surface area goes from 80 to 540 $m^2 \cdot g^{-1}$ (Figure 7). In the absence of microporosity, these surface areas can be

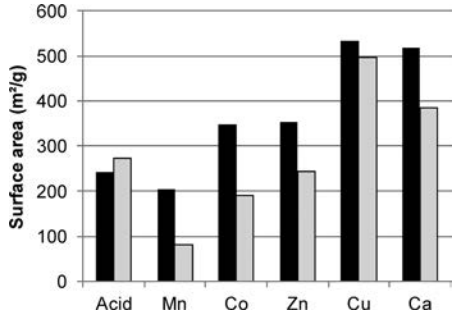

Figure 7. Surface areas of aerogel of HG alginate (black bars) or LG alginate (gray bars) with various cations.

attributed to the outer surface of the fibrils. Alginate HG generally produces samples with higher surface area compared with alginate LG. A difference around 100 $m^2 \cdot g^{-1}$ is observed except for acidic and copper gels where the values are very close. Moreover, the surface area seems to be strongly related to the gelling agent giving a ranking which is independent of the alginate if we exclude the case of acidic gelling.

In view of Figure 6 displaying fiber morphologies in all systems, the morphology studied by SAXS should be related to a more local scale within fibers.

As far as the preparations of highly dispersed materials are needed, for example, for adsorption, catalysis, and remediation in liquid or gas phase applications, the higher surface areas are obtained for the systems that display the fibrillar organization resulting from the higher intermacromolecular interaction and structuring. Figure 8 evidences the correlation between the

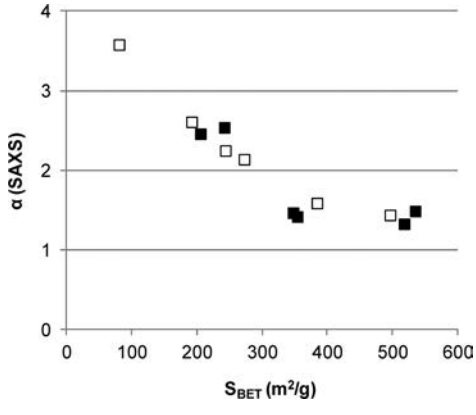

Figure 8. Relation between surface area of aerogel of alginate HG (filled symbols) or LG (empty symbols) with various cations and the scattering exponent α (from SAXS measurements at low q values).

textural properties of the aerogels and the scattering exponent α (SAXS) whatever the G content of the alginate.

CONCLUSIONS

The morphologies of several ionotropic alginate hydrogels and aerogels were investigated according to the nature of the divalent cation (Mn^{2+}, Co^{2+}, Zn^{2+}, Cu^{2+}) and the guluronic fraction of the alginate. Copper cations seem to interact strongly with both mannuronic and guluronic residues and induce a comparable fibrillar morphology whatever the guluronic content. With cobalt and zinc, the guluronic fraction impacts the hydrogel morphology. Mn and acidic hydrogels display the nonfibrillar morphology that could be due to an absence of cooperative interchain associations for all investigated alginate types. In the size range investigated by SAXS (∼10−200 Å), the structure of aerogels is found to be inherited from the morphology of the parent hydrogel, whatever the initial structural regime (fibrillar junctions gels or gels with multiple junction nature). The surface areas and thus the overall performance of such materials as catalysts are in close relation with the structural regime exhibited by aerogels.

ASSOCIATED CONTENT

Supporting Information

Complete characterization of the alginates, mass analysis of aerogel samples, the scattering exponent in the low-q asymptotic regime as function of cation nature, alginate structure, and hydrogel/aerogel physical state, and the fibril diameter estimated through the maxima of Kratky plots are reported. This material is available free of charge via the Internet at http://pubs.acs.org.

AUTHOR INFORMATION

Corresponding Author

E-mail: quignard@enscm.fr. Fax: (33) 4 67 16 34 70.

ACKNOWLEDGMENTS

We gratefully acknowledge Didier Cot (IEMM) for the scanning electron microscopy. SAXS was performed at ESRF during experiment IN-728 from March 31, 2010 to April 1, 2010. It is a pleasure to acknowledge the BM2-D2AM beamline staff and more specifically Dr. Cyrille Rochas for his invaluable help during pre-experiment formalities, SAXS experiments, and data treatment.

REFERENCES

(1) McHugh, D. J. In *A Guide to the Seaweed Industry*; FAO Fisheries Technical Paper: Rome, 2003; p 27.

(2) Barbotin, J. N.; Nava Saucedo, J. E. In *Polysaccharides*, Dumitriu, S., Ed.; Marcel Dekker: New York, 1998; p 749.

(3) Sime, W. J. In *Food Gels*; Harris, P., Ed.; Elsevier: Amsterdam, 1990; p 53.

(4) Chen, J. P.; Hong, L.; Wu, S.; Wang, L. *Langmuir* **2002**, *18*, 9413−9421.

(5) Tønnesen, H. H.; Karlsen, J. *Drug Dev. Ind. Pharm.* **2002**, *28*, 621−630.

(6) Grant, G. T.; Morris, E. R.; Rees, D. A.; Smith, P. J. C. *FEBS Lett.* **1973**, *32*, 195−197.

(7) Morris, E. R.; Rees, D. A.; Thorn, D.; Boyd, J. *Carbohydr. Res.* **1978**, *66*, 145−154.

(8) Morris, E. R.; Rees, D. A.; Young, G. *Carbohydr. Res.* **1982**, *108*, 181−195.

(9) Thom, D. T.; Grant, G. T.; Morris, E. R.; Rees, D. A. *Carbohydr. Res.* **1982**, *100*, 29−42.

(10) Lu, L.; Liu, X.; Qian, L.; Tong, Z. *Polym. J.* **2003**, *35*, 804−809.

(11) Cesaro, A.; Delben, F.; Paoletti, S. *J. Chem. Soc., Faraday Trans. 1* **1988**, *84*, 2573−2584.

(12) Ouwerx, C.; Velings, N.; Mestdagh, M. M.; Axelos, M. A. V. *Polym. Gels Networks* **1998**, *6*, 393−408.

(13) Draget, K. I.; Skjåk-Braek, G.; Smidsrød, O. *Carbohydr. Polym.* **1994**, *25*, 31−38.

(14) Wang, X.; Spencer, H. G. *Polymer* **1998**, *39*, 2759−2764.

(15) Siew, C. K.; Williams, P. A.; Young, N. W. G. *Biomacromolecules* **2005**, *6*, 963−969.
(16) Sterling, C. *Biochim. Biophys. Acta* **1957**, *26*, 186−197.
(17) Yokoyama, F.; Achife, E. C.; Matoka, J.; Shimamura, K.; Yamashita, Y.; Monobe, K. *Polymer* **1991**, *32*, 2911−2916.
(18) Yokoyama, F.; Achife, E. C.; Takahira, K.; Yamashita, Y.; Monobe, K. *J. Macromol. Sci. Phys.* **1992**, *B31*, 463.
(19) Mongar, I. L.; Wassermann, A. *J. Chem. Soc.* **1952**, 492−497.
(20) Stokke, B. T.; Draget, K. I.; Smidsrød, O.; Yuguchi, Y.; Urakawa, H.; Kajiwara, K. *Macromolecules* **2000**, *33*, 1853−1863.
(21) Yuguchi, Y.; Urakawa, H.; Kajiwara, K.; Draget, K. I.; Stokke, B. T. *J. Mol. Struct.* **2000**, *554*, 21−34.
(22) Draget, K. I. *Annu. Trans. - Nord. Rheol. Soc.* **2001**, *8/9*, 149.
(23) Draget, K. I.; Stokke, B. T.; Yuguchi, Y.; Urakawa, H.; Kajiwara, K. *Biomacromolecules* **2003**, *4*, 1661−1668.
(24) Maki, Y.; Ito, K.; Hosoya, N.; Yoneyama, C.; Furusawa, K.; Yamamoto, T.; Dobashi, T.; Sugimoto, Y.; Wakabayashi, K. *Biomacromolecules* **2011**, *12*, 2145−2152.
(25) Robitzer, M.; David, L.; Rochas, C.; Di Renzo, F.; Quignard, F. *Langmuir* **2008**, *24*, 12547−12552.
(26) Towler, J. P.; Oroskar, A. R.; Amity, S. E. *Environ. Prog.* **2004**, *23*, 334−341.
(27) Quignard, F.; Di Renzo, F.; Guibal, E. *Top. Curr. Chem.* **2010**, *294*, 165−197.
(28) Grasdalen, H.; Larsen, B.; Smidsrød, O. *Carbohydr. Res.* **1979**, *68*, 23−31.
(29) Grasdalen, H. *Carbohydr. Res.* **1983**, *118*, 255−260.
(30) Horga, R.; Di Renzo, F.; Quignard, F. *Appl. Catal., A* **2007**, *325*, 251−255.
(31) Valentin, R.; Horga, R.; Bonelli, B.; Garrone, E.; Di Renzo, F.; Quignard, F. *Biomacromolecules* **2006**, *7*, 877−882.
(32) Draget, K. I.; Skjåk-Bræk, G.; Stokke, B. T. *Food Hydrocolloids* **2006**, *20*, 170−175.
(33) Mackie, W.; Perez, S.; Rizzo, R.; Taravel, F.; Vignon, M. *Int. J. Biol. Macromol.* **1983**, *5*, 329−341.
(34) Perić, L.; Pereira, C. S.; Perez, S.; Hünenberger, P. H. *Mol. Simul.* **2008**, *34*, 421−446.
(35) Valentin, R.; Molvinger, K.; Quignard, F.; Di Renzo, F. *Macromol. Symp.* **2005**, *222*, 93−101.
(36) Rouquerol, F.; Rouquerol, J.; Sing, K. In *Adsorption by Powders and Porous Solids*; Academic Press: San Diego, 1999; p 18.